Electronic Supplementary Material (ESI) for Green Chemistry.

Cobalt-doped Manganese (III) oxide cathode materials with enhanced electrochemical performance for aqueous zinc-ion batteries

Zixiang Zhou[a], Jianbo Tong[a]*, Jiale Guo[a], Shaofeng Guo[a], Shuhan Liu[a], Zhipeng Qin[a], Muxuan Luo[b], Chao Wang[a], Shuling Liu[a]*

[a] *Department of Chemistry and Chemical Engineering, Shaanxi Collaborative Innovation Center of Industrial Auxiliary Chemistry & Technology, Key Laboratory of Auxiliary Chemistry and Technology for Chemical Industry, Ministry of Education, Shaanxi University of Science and Technology, Xi'an, Shaanxi 710021, China*

[b] *State Key Laboratory of Advanced Processing and Recycling of Non-ferrous Metals, Lanzhou University of Technology, Lanzhou 730050, China*

*Corresponding author.

E-mail address: liushuling@sust.edu.cn

jianbotong@aliyun.com

Chemicals

The following reagents were used without further purifications. Manganese nitrate tetrahydrate ($Mn(NO_3)_2 \cdot 4H_2O$, AR, 98.0%), Cobalt nitrate hexahydrate ($Co(NO_3)_2 \cdot 6H_2O$), Glycerol ($C_3H_8O_3$, AR, 99%), Isopropyl Alcohol (C_3H_8O, AR, 99%), manganese sulfate tetrahydrate ($MnSO_4 \cdot 4H_2O$, AR, 98.0%), zinc sulfate heptahydrate ($ZnSO_4 \cdot 7H_2O$, AR, 98.0%), and doubly distilled water.

Material characterizations

Crystallographic phases of the samples are assessed using X-ray diffraction (XRD) employing a Bruker D8 Advance instrument in Bragg-Brentano geometry with a Cu target (λ = 0.154 nm). X-ray photoelectron spectroscopy (XPS) measurements are performed using an AXIS SUPRA instrument (Renishaw-invia). Field emission scanning electron microscopy (FE-SEM) at an accelerating voltage of 10 kV equipped with energy-dispersive X-ray spectroscopy (EDS) (Xplore-30, Oxford) is employed to observe sample morphologies. Raman spectroscopy measurements are conducted using a Renishaw Invia Raman spectroscope. Transmission electron microscopy (TEM), High-resolution transmission electron microscopy (HR-TEM), and selected area electron diffraction (SAED) patterns are obtained utilizing the FEI Tecnai G2 F20 instrument with an acceleration voltage of 200 kV.

Electrochemical characterizations

The cathode of the ZIBs is fabricated using active material, acetylene black as the conductive agent, and polyvinylidene fluoride as the binder (with a weight ratio of 7:2:1), and N-methyl-2-pyrrolidone is utilized as the solvent during the process of ink slurry preparation. After continuous stirring, the resulting slurry is coated onto a

stainless steel circular mesh with a diameter of 12 mm, followed by drying in a vacuum oven at 80 ℃ for 12 h. The active material loading is approximately 2 mg cm^{-2}. The electrochemical analysis of all samples is performed using a CR2032 coin cell with zinc foil as the negative electrode, glass fiber as the separator, and 2 M $ZnSO_4$ + 0.2 M $MnSO_4$ aqueous solution as the electrolyte. Cyclic voltammetry (CV) and electrochemical impedance spectroscopy (EIS) are conducted using CHI660E or PARSTAT MC potentiostats. Unless specified otherwise, all potentials are referenced to Zn/Zn^{2+}. The CV are performed within the range of 1-1.85 V at a scan rate of 0.1 mV s^{-1}, while EIS measurements are carried out across a frequency spectrum from 10^5 to 0.01 Hz, with an alternating potential amplitude of 5 mV. A battery test system (LAND MTI-5 V 10 mA) is utilized to assess the cycling and charge–discharge characteristics of the coin cells. The galvanostatic intermittent titration technique (GITT) involves a series of galvanostatic discharge pulses (10 minutes at 100 mA g^{-1} followed by a 30-minute rest) within the potential range of 1-1.85 V.

Density functional theory calculations

Calculations are conducted within the density functional theory (DFT) framework, employing the projected enhanced wave method and implemented using the Vienna Ab initio Simulation Package (VASP). The core separation and valence electron interactions are described by projected added waves (PAW), and the local density is described using the generalized gradient approximation (GGA) based on exchange correlation energy PBE. Brillouin zone divisions are sampled using Monkhorst-Pack method. ENCUT= 400 eV is selected as the cutoff energy value for the calculation.

The K points of dimensions 1×1×1-3×3×1 are generated by optimizing the convergence sampling in the calculation of the diffusion barrier and the mechanical strength, respectively. The precision values for electron and ion relaxation convergence are 1.0×10^{-4} eV and 1.0×10^{-3} eV, and the force convergence criterion is 0.02 eV/Å.

Energy Density and Power Density

The energy density and power density were obtained by the following equations:

$$E = \int_0^{\Delta t} \frac{V \times i}{m} dt$$

$$P = \frac{E}{1000 \times \Delta t}$$

where E (Wh kg^{-1}) is the energy density, P is the power density (kW kg^{-1}), V (V), i (mA), m (g) and Δt (h) represent the working potential, discharging current, the mass loading of the cathode and the discharging time, respectively.

Diffusion Coefficient

The diffusion coefficient (D) is obtained from the following equation,

$$D = \frac{4L^2}{\pi\tau}\left(\frac{\Delta Es}{\Delta Et}\right)$$

where τ (s) is the constant current pulse time. The L is diffusion length (cm) of Zn^{2+} and H^+ which is equal to thickness of electrode. The ΔEs is the steady-state voltage change caused by the current pulse. The ΔEt are voltage changes during the constant current pulse.

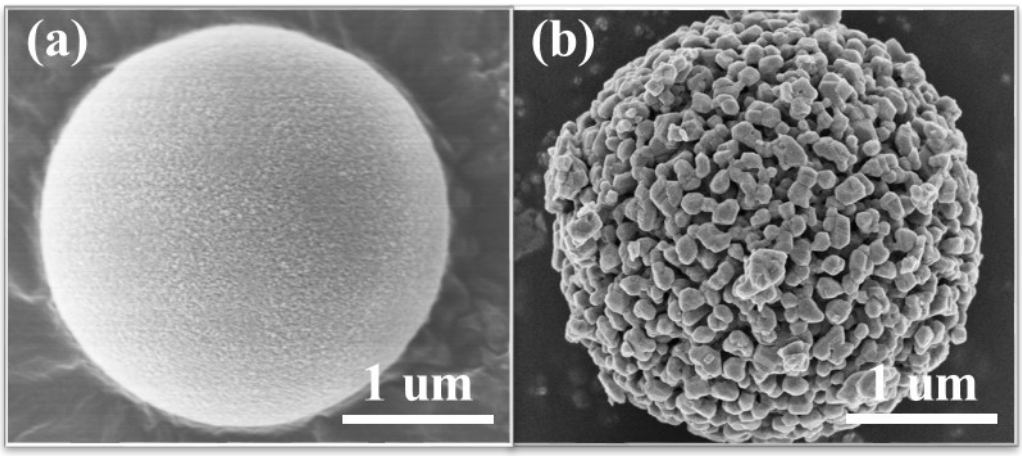

Fig. S1. SEM images of the (a) Mn glycerate and (b) Mn_2O_3.

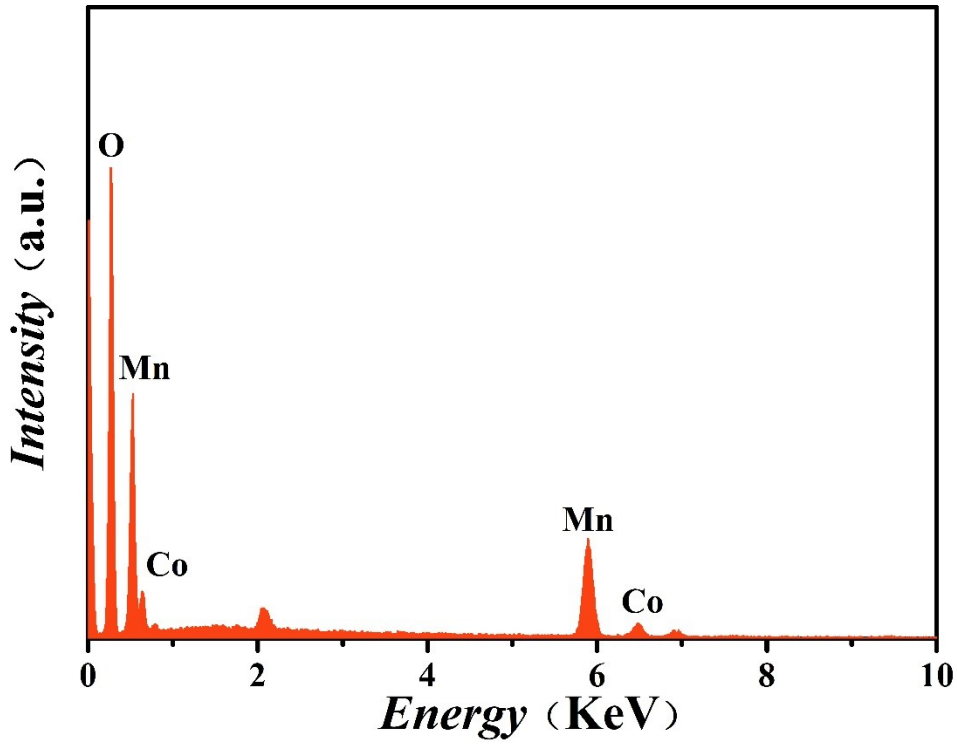

Fig. S2. EDS spectrum of the Co-Mn_2O_3.

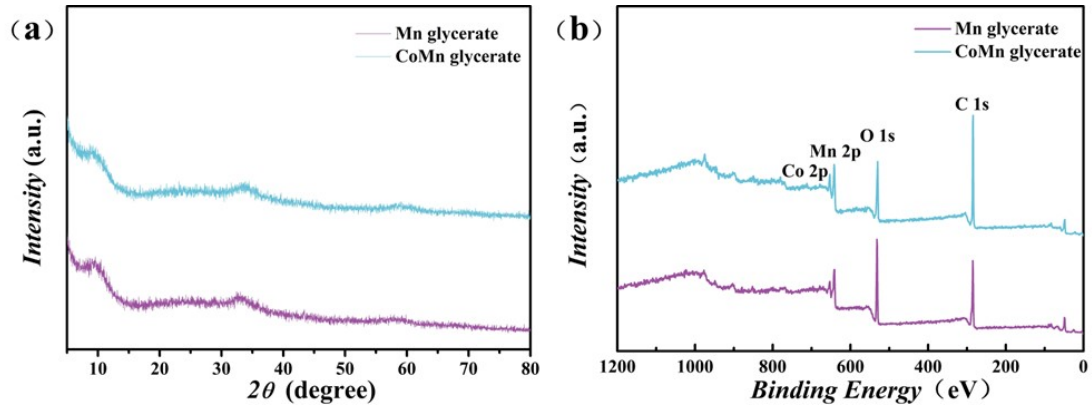

Fig. S3. (a) XRD patterns of the Mn glycerate and CoMn glycerate; (b) XPS survey spectra of the Mn glycerate and CoMn glycerate.

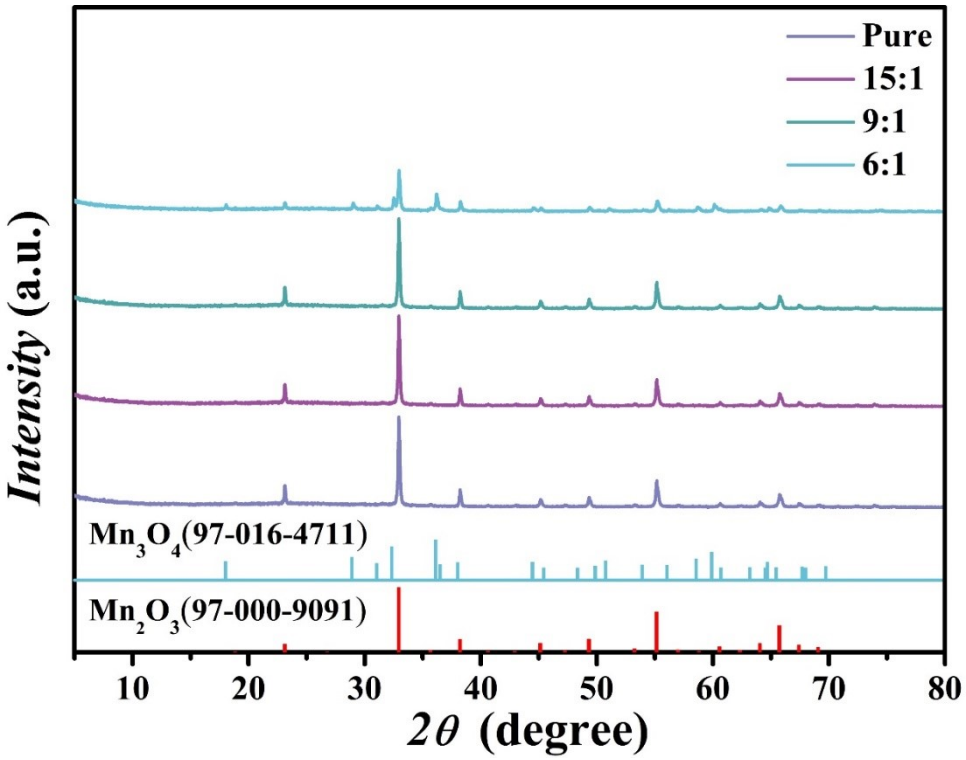

Fig. S4. XRD patterns of the Co-doped Mn_2O_3 at varying proportions.

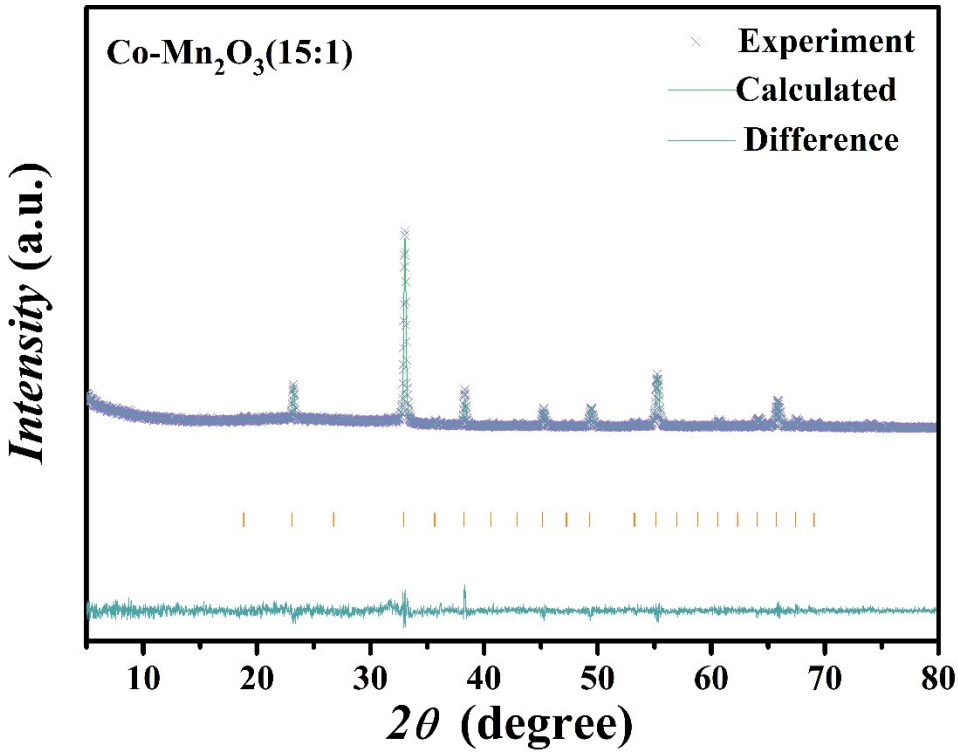

Fig. S5. Rietveld refinement of XRD patterns of the Co-Mn_2O_3(15:1).

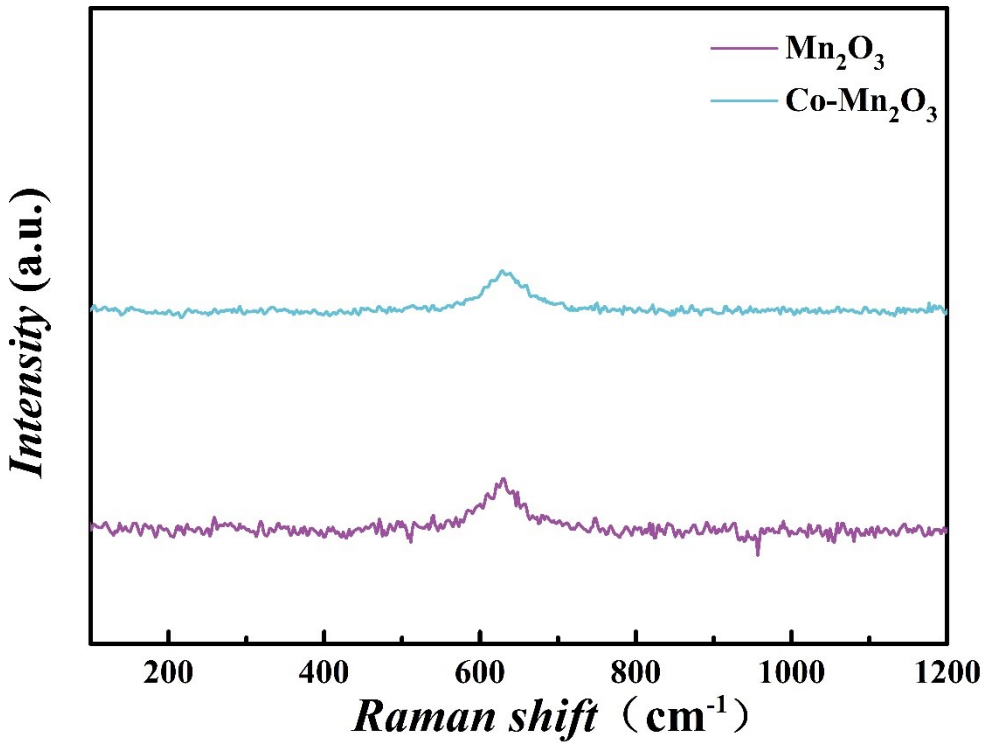

Fig. S6. Raman spectra of the Mn_2O_3 and Co-Mn_2O_3.

Table 1. XRD refinement parameters and optimized results of the Co-doped Mn_2O_3 at varying proportions.

Samples	Mn_2O_3	Co-Mn_2O_3(15:1)	Co-Mn_2O_3(9:1)
		Cu Kα	
		Cubic la-3	
a	9.4119 Å	9.3964 Å	9.3822 Å
b	9.4119 Å	9.4065 Å	9.3951 Å
c	9.4119 Å	9.3877 Å	9.3735 Å
α	90°	90°	90°
β	90°	90°	90°
γ	90°	90°	90°
Cell volume	833.7423 $Å^3$	829.7528 $Å^3$	826.2431 $Å^3$
Rwp	6.82%	7.33%	7.49%

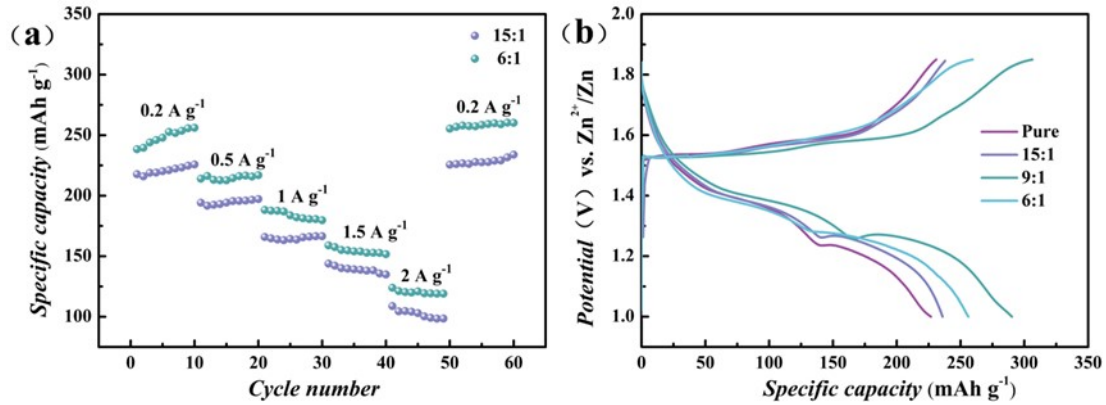

Fig. S7. (a) Rate performances of Co-doped Mn_2O_3 at varying proportions; (b) Charge and discharge curves of Co-doped Mn_2O_3 at varying proportions at 0.2 A g^{-1}.

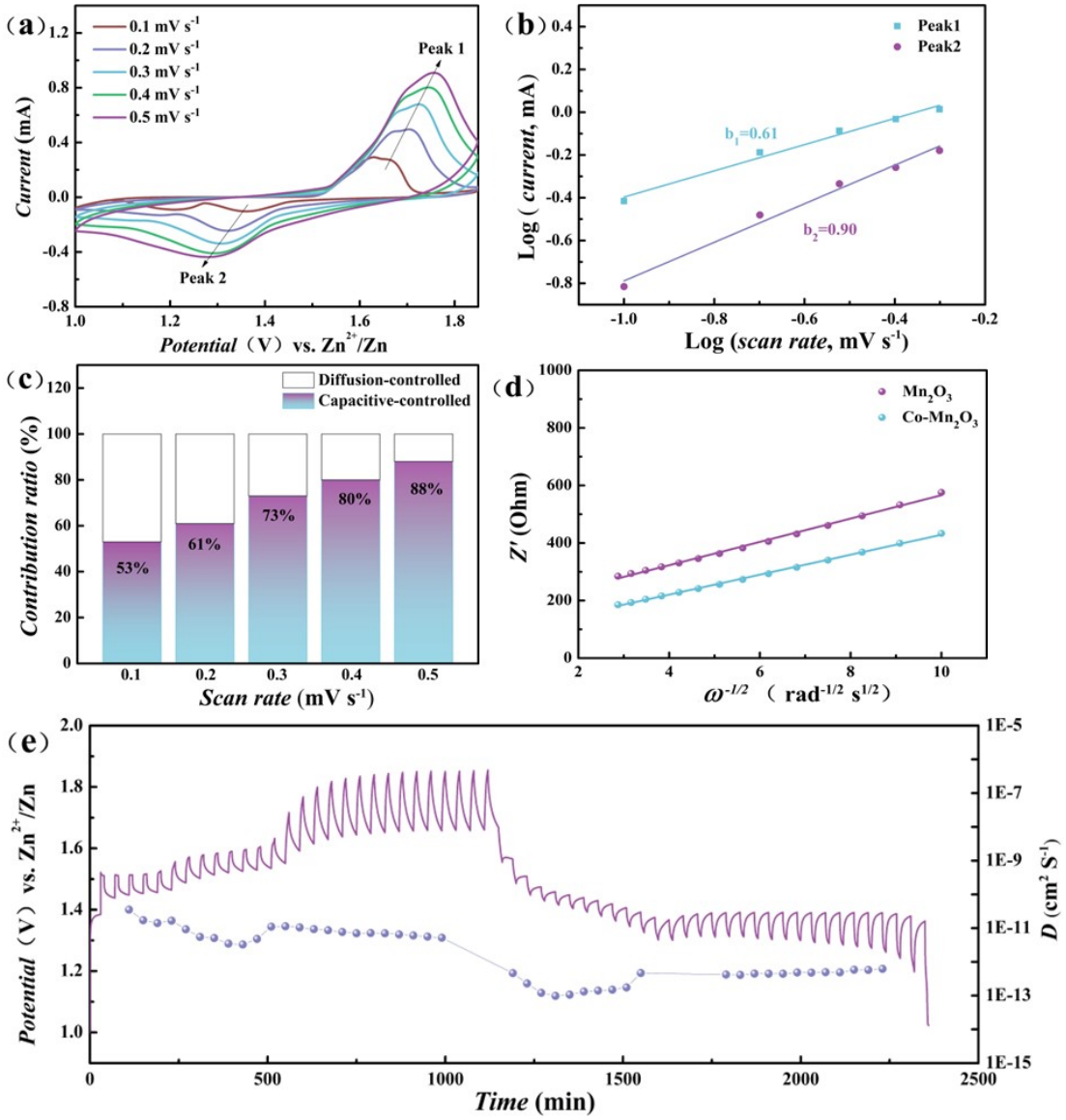

Fig. S8. (a) CV curves of Mn_2O_3 ranging from 0.1 to 0.9 mV s^{-1}; (b) Log (peak current) versus log (scan rate) plot of Mn_2O_3; (c) Contribution of the capacitive-controlled process to the capacity of Mn_2O_3; (d) Plots of Z' versus $\omega^{-1/2}$ of the Mn_2O_3 and Co-Mn_2O_3; (e) GITT plot and the associated diffusivity coefficients during the charge-discharge process of Mn_2O_3.

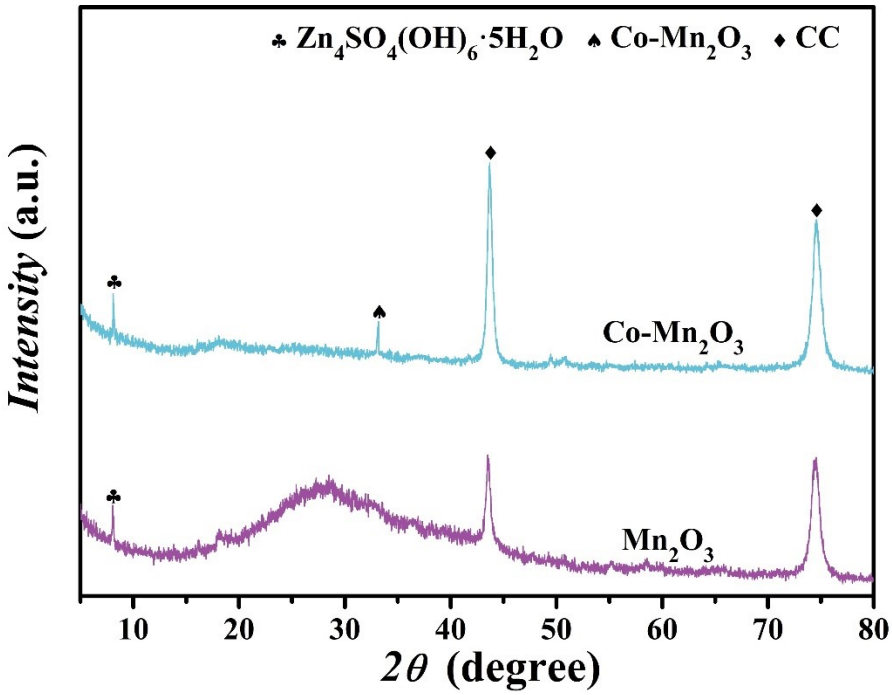

Fig. S9. XRD pattern of the Mn_2O_3 and Co-Mn_2O_3 following 100 cycles of charge and discharge.

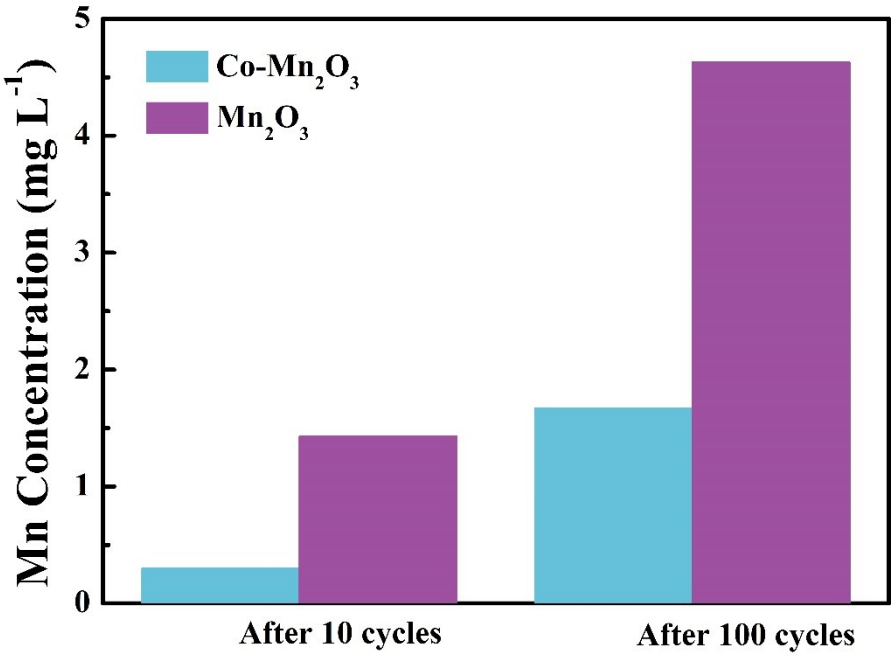

Fig. S10. ICP measurement of manganese dissolution of the Mn_2O_3 and Co-Mn_2O_3 in 2 M $ZnSO_4$.

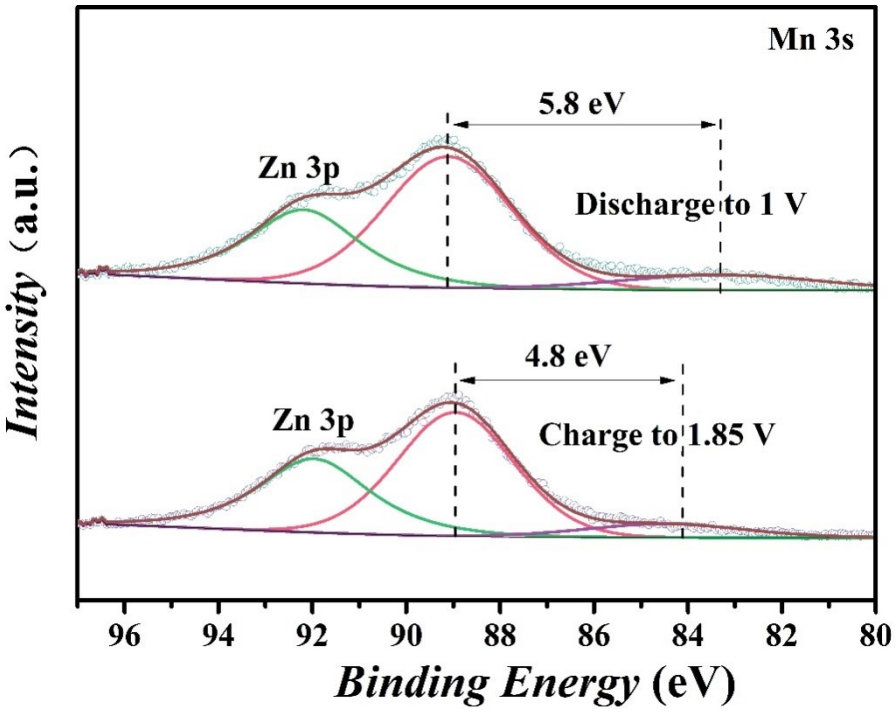

Fig. S11. XPS spectra of Mn 3s region at the charging and discharging states.

Table S2. Performance comparison of aqueous ZIBs with manganese oxide-based materials as cathodes.

Cathode material	Electrolyte	Specific capacity	Capacity retention	Ref.
Co-Mn_2O_3	2 M $ZnSO_4$+ 0.2 M $MnSO_4$	289.7 mA h g^{-1} at 0.2 A g^{-1}	84.6% after 1000 cycles at 2 A g^{-1}	This work
NM20	2 M $ZnSO_4$+ 0.2 M $MnSO_4$	252 mA h g^{-1} at 0.1 A g^{-1}	85.6% after 2500 cycles at 1 A g^{-1}	[1]
α-Mn_2O_3	2 M $ZnSO_4$+ 0.2 M $MnSO_4$	225 mA h g^{-1} at 0.05 A g^{-1}	53.3% after 1700 cycles at 2 A g^{-1}	[2]
Mn_2O_3@PPy	3 M $ZnSO_4$+ 0.5 M $MnSO_4$	290.6 mA h g^{-1} at 0.2 A g^{-1}	82.2% after 300 cycles at 0.1 A g^{-1}	[3]
O_{cu}-Mn_2O_3	3 M $ZnSO_4$+ 0.1 M $MnSO_4$	241 mA h g^{-1} at 0.1 A g^{-1}	88% after 600 cycles at 1 A g^{-1}	[4]
F-MO	2 M $ZnSO_4$+ 0.2 M $MnSO_4$	288 mA h g^{-1} at 0.1 A g^{-1}	96% after 200 cycles at 0.2 A g^{-1}	[5]
MnO_2 @MXene	2 M $ZnSO_4$+ 0.2 M $MnSO_4$	184 mA h g^{-1} at 0.05 A g^{-1}	84.5% after 1000 cycles at 0.1 A g^{-1}	[6]
HCM	2 M $ZnSO_4$+ 0.3 M $MnSO_4$	341 mA h g^{-1} at 0.2 A g^{-1}	87% after 3500 cycles at 2 A g^{-1}	[7]
ε- MnO_2@N	2 M $ZnSO_4$+ 0.5 M $MnSO_4$	183.4 mA h g^{-1} at 0.5 A g^{-1}	83% after 1000 cycles at 5 A g^{-1}	[8]
δ- MnO_2	1 M $ZnSO_4$	252 mA h g^{-1} at 0.083 A g^{-1}	43% after 100 cycles at 0.083 A g^{-1}	[9]
$ZnMn_2O_4$/NG	1 M $ZnSO_4$+ 0.05 M $MnSO_4$	232 mA h g^{-1} at 0.1 A g^{-1}	97.4% after 2500 cycles at 1 A g^{-1}	[10]
ZMO/CNTs	1 M $ZnSO_4$+ 0.1 M $MnSO_4$	220.3 mA h g^{-1} at 0.1 A g^{-1}	97.0% after 2000 cycles at 3 A g^{-1}	[11]
α-MnO_2/CNT HMs	2 M $ZnSO_4$+ 0.1 M $MnSO_4$	296 mA h g^{-1} at 0.2 A g^{-1}	No decreasing after 100 cycles at 0.2 A g^{-1}	[12]
Ti-MnO_2	3 M $Zn(CF_3SO_3)_2$ + 0.1 M $Mn(CF_3SO_3)_2$	259 mA h g^{-1} at 0.1 A g^{-1}	80% after 4000 cycles at 1 A g^{-1}	[13]

References

1. D. Zhang, J. Cao, X. Zhang, N. Insin, S. Wang, J. Han, Y. Zhao, J. Qin and Y. Huang, *Advanced Functional Materials*, 2021, **31**, 2009412.
2. M. Mao, X. Wu, Y. Hu, Q. Yuan, Y.-B. He and F. Kang, *Journal of Energy Chemistry*, 2021, **52**, 277-283.
3. K. Cai, S.-h. Luo, L. Qian, X. Meng, S.-x. Yan, J. Guo, Q. Wang, X.-b. Ji and X.-y. Zhou, *Journal of Power Sources*, 2023, **564**, 232854.
4. N. Liu, X. Wu, Y. Yin, A. Chen, C. Zhao, Z. Guo, L. Fan and N. Zhang, *ACS applied materials & interfaces*, 2020, **12**, 28199-28205.
5. D. Wang, Z. Liu, X.-W. Gao, Q. Gu, L. Zhao and W.-B. Luo, *Journal of Energy Storage*, 2023, **72**, 108740.
6. L. Wu, Y. Mei, Y. Liu, W. Xu, M. Zhang, Y. Dong and Z.-S. Wu, *Chemical Engineering Journal*, 2023, **459**, 141662.
7. S. Luo, J. Xu, B. Yuan, L. Chen, L. Xu, R. Zheng, Y. Wang, M. Zhang, Y. Lu and Y. Luo, *Carbon*, 2023, **214**, 118334.
8. Y. Zhang, Y. Liu, Z. Liu, X. Wu, Y. Wen, H. Chen, X. Ni, G. Liu, J. Huang and S. Peng, *Journal of Energy Chemistry*, 2022, **64**, 23-32.
9. M. H. Alfaruqi, J. Gim, S. Kim, J. Song, D. T. Pham, J. Jo, Z. Xiu, V. Mathew and J. Kim, *Electrochemistry Communications*, 2015, **60**, 121-125.
10. L. Chen, Z. Yang, H. Qin, X. Zeng and J. Meng, *Journal of power sources*, 2019, **425**, 162-169.
11. F. Gao, B. Mei, X. Xu, J. Ren, D. Zhao, Z. Zhang, Z. Wang, Y. Wu, X. Liu

and Y. Zhang, *Chemical Engineering Journal*, 2022, **448**, 137742.

12. Y. Liu, X. Chi, Q. Han, Y. Du, J. Huang, Y. Liu and J. Yang, *Journal of Power Sources*, 2019, **443**, 227244.

13. S. Lian, C. Sun, W. Xu, W. Huo, Y. Luo, K. Zhao, G. Yao, W. Xu, Y. Zhang and Z. Li, *Nano Energy*, 2019, **62**, 79-84.